Commun. Theor. Phys. (Beijing, China) **49** (2008) pp. 771–776

Vol. 49, No. 3, March 15, 2008

Fano Effect in T-Shaped Double Quantum Dot Structure with Decoherence Effect*

GAO Wen-Zhu, GONG Wei-Jiang, ZHENG Yi-Song,† LIU Yu, and LÜ Tian-Quan

Department of Physics, Jilin University, Changchun 130023, China

(Received March 16, 2007; Revised May 8, 2007)

Abstract *By introducing a floating lead to mimic the decoherence mechanism, the Fano effect in the linear conductance spectrum of a T-shaped double quantum dot structure is studied. We find that even in the case that the self-energy arising from the decoherence mechanism is much smaller than the coupling strength between the connected quantum dot and the conducting lead, the Fano lineshape can be largely destroyed. In addition, the decoherence renders the high-order electron transmission paths unimportant to contributing to the Fano lineshape.*

PACS numbers: 73.63.Kv, 73.21.La, 73.23.Ra, 73.63.Nm
Key words: quantum dot, conductance, Fano effect

1 Introduction

Fano effect,[1] stemming from the quantum interference between the resonant and nonresonant processes, manifests itself as an asymmetric lineshape in many observable spectra of various physical fields. The recent observation of the Fano effect in the electronic transport spectrum in QD structure confirms the quantum interference of the electron waves in the mesoscopic scale.[2−4] Unlike the conventional one, the Fano effect in the quantum dot (QD) system has its peculiarity in that its key parameters can be readily adjusted. Therefore, there has been much interest to investigate theoretically the Fano effect in the QD structure.[5−10]

Although most electronic transport properties through QD structures are dominated by quantum coherence, the decoherence mechanism always exists and influences the electronic transport to some extent. Therefore, it is a practical issue to study to what extent the Fano lineshape in the electronic transport spectrum survives in the presence of the decoherence effect. There are many decoherence mechanisms, e.g., the electron-phonon interaction[11,12] and the electron-electron interaction.[13] They destroy the coherent electron transport in different ways. However, a general and simple approach to study the decoherence effect is to introduce a floating lead coupling directly to QD. The term "floating" indicates that such a lead does not conduct a net current flow. In other words, the floating lead is just a voltage probe. When an electron enters such a lead, another electron in the lead will certainly go into the QD to cancel the charge transfer. But the electron phase is randomized in such a process to give rise to the decoherence.[14]

In the present paper, our purpose is to study the influence of the decoherence on the Fano lineshape of the electronic conductance spectrum through QD structure. Following the simple physical picture depicted above, we consider a T-shaped double QD structure coupled to form a mesoscopic circuit to conduct the current flow. Thus the different transmission paths are achieved for the Fano interference. More importantly, to mimic the decoherence mechanism we introduce one foating lead coupling to the lateral QD. By adjusting the coupling strength between the QD and the floating lead, the influence of the decoherence on the Fano effect can be studied in detail.

The rest of the paper is organized as follows. In Sec. 2, the model Hamiltonian to describe electron behavior in the double QD system is introduced first. Next, a formula for linear conductance is derived by means of the nonequilibrium Green function technique. Then, a Feynman path analysis is performed for the electron transmission amplitude. In Sec. 3, the calculated results regarding the conductance spectrum are shown. Then a discussion on the numerical results, particularly those concerning the change of the Fano lineshape of the linear conductance, is given. Finally, the main results are summarized in Sec. 4.

2 Theoretical Model

The T-shaped double QD structure with the extra dot-lead coupling to the dangling QD (QD-2) is schematically illustrated in Fig. 1. The electron motion in this system can be well described by a generalized Anderson impurity Hamiltonian that reads

$$H = H_C + H_D + H_T + H_{e-e}\,, \tag{1}$$

where H_C and H_D are the Hamiltonians in the three leads and the QDs, respectively, H_T describes the electron tunneling between the leads and the QDs, and H_{e-e} denotes the many-body terms due to the electron interaction. They are given by

$$H_C = \sum_{k\sigma\alpha\in L,R,D} \varepsilon_{k\alpha} c^{\dagger}_{k\sigma\alpha} c_{k\sigma\alpha}\,, \quad H_D = \sum_{\sigma,j=1}^{2} \varepsilon_j d^{\dagger}_{j\sigma} d_{j\sigma} + \sum_{\sigma} (t_1 d^{\dagger}_{2\sigma} d_{1\sigma} + \text{H.c.})\,,$$

*The project supported by National Natural Science Foundation of China under Grant No. 10774055
†Author to whom correspondence should be addressed, E-mail address: zys@mail.jlu.edu.cn

$$H_T = \sum_{k\sigma\beta\in L,R} (V_{1\beta} c^\dagger_{k\sigma\beta} d_{1\sigma} + \text{H.c.}) + \sum_{k\sigma D} (V_{2D} c^\dagger_{k\sigma D} d_{2\sigma} + \text{H.c.}) , \quad H_{e-e} = \sum_{j=1}^{2} U_j n_{j\uparrow} n_{j\downarrow} . \tag{2}$$

In the above equations, $c^\dagger_{k\sigma\alpha}$ and $d^\dagger_{j\sigma}$ ($c_{k\sigma\alpha}$ and $d_{j\sigma}$) are operators to create (annihilate) an electron of the continuous state k in the leads and QD-j, respectively. $\alpha = L$ or R represents the lead coupled to QD-1 and $\alpha = D$ denotes the extra lead coupled to QD-2, and σ is the spin index. $\varepsilon_{k\alpha}$ and ε_j denote the corresponding energy levels. t_1 is the interdot coupling coefficient between the two QDs. V_L and V_R denote the tunneling matrix elements between QD-1 and the leads, which are all simplified as constants. $n_{j\sigma} = d^\dagger_{j\sigma} d_{j\sigma}$ with $\sigma = \uparrow$ or $\downarrow$ are the electron number operator in QD-j. U_j indicates the strength of intradot Coulomb repulsion of the electrons in QD-j. All the interdot electron interactions are ignored since they are usually much smaller than the intradot interactions due to the screening effect. In addition, V_{2D} denotes the tunneling matrix element between QD-2 and the down lead. Here, the down lead is considered as the floating lead.

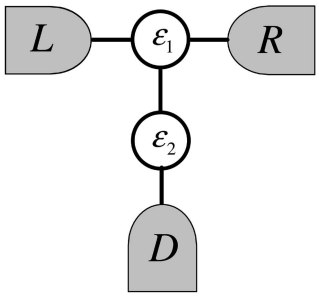

Fig. 1 A schematic illustration of the T-shaped double QDs (denoted by ε_1 and ε_2) with the floating lead (denoted by D) coupling to the lateral QD. A current flow occurs from the left lead to the right one (denoted by L and R respectively) by tunneling through the QDs.

In order to study the electron transport properties in the system, the linear conductance between the left and the right leads should be calculated. The linear conductance associated with the electron transmission function can be expressed in terms of Green functions. It takes a form as[15,16]

$$\mathcal{G} = \frac{e^2}{h} \sum_\sigma T_\sigma(\omega)|_{\omega=\varepsilon_F} , \tag{3}$$

where $T_\sigma(\omega)$ is the transmission function, and it is expressed as[17]

$$T_\sigma(\omega) = \Gamma^L_{11} \Gamma^R_{11} |G^r_{11,\sigma}(\omega)|^2 . \tag{4}$$

We need to point out that this formula is valid only in the situation of $I_D = 0$, which just follows the definition of the floating lead. Γ^L describes the coupling strength between QD-1 and the left lead, which is defined as $[\Gamma^L]_{11} = 2\pi V_{1L} V^*_{1L} \rho_L(\omega)$. We will ignore the ω-dependence of Γ^L since the electron density of states in the left lead, $\rho_L(\omega)$, can be usually viewed as a constant. Similarly, we can define $[\Gamma^R]$ and $[\Gamma^D]$. In Eq. (4) the retarded and advanced Green functions in Fourier space are involved. They are defined as follows: $G^r_{jl,\sigma}(t) = -\mathrm{i}\theta(t)\langle\{d_{j\sigma}(t), d^\dagger_{l\sigma}\}\rangle$ and $G^a_{jl,\sigma}(t) = \mathrm{i}\theta(-t)\langle\{d_{j\sigma}(t), d^\dagger_{l\sigma}\}\rangle$, where $\theta(x)$ is the step function. The Fourier transforms of the Green functions can be performed via $G^{r(a)}_{jl,\sigma}(\omega) = \int_{-\infty}^{\infty} G^{r(a)}_{jl,\sigma}(t)\, \mathrm{e}^{\mathrm{i}\omega t} \mathrm{d}t$. These Green functions can be solved by the equation-of-motion method. We introduce an alternative notation $\langle\langle A|B\rangle\rangle^x$ with $x = r$ or a to denote the Green functions in Fourier space. For example, $G^r_{jl,\sigma}(\omega)$ is identical to $\langle\langle d_{j\sigma}|d^\dagger_{l\sigma}\rangle\rangle^r$. The solution of Green functions is crucial for the calculation of the conductance. To do so we employ the equation-of-motion method of the Green functions. However, if we incorporate the electron interaction terms in the Hamiltonian, it is impossible to obtain exact solutions of the Green functions. In such a case, we have to truncate the equations of motion of the Green functions at some order to obtain the approximate solutions of the Green functions. To begin with, we notice that the Green functions obey the following equation,[18]

$$(\omega \pm \mathrm{i}0^+)\langle\langle A|B\rangle\rangle^{r(a)} = \langle\{A, B\}\rangle + \langle\langle [A, H]|B\rangle\rangle^{r(a)} . \tag{5}$$

Starting from Eq. (5), we can first derive the equation of motion of the retarded Green function $\langle\langle d_{j\sigma}|d^\dagger_{l\sigma}\rangle\rangle^r$, which yields

$$\begin{aligned} &(z - \varepsilon_j + \mathrm{i}\Gamma_{jj})\langle\langle d_{j\sigma}|d^\dagger_{l\sigma}\rangle\rangle^r \\ &= \delta_{jl} + t_{j-1}(1-\delta_{j1})\langle\langle d_{j-1\sigma}|d^\dagger_{l\sigma}\rangle\rangle^r \\ &\quad + t^*_j(1-\delta_{j2})\langle\langle d_{j+1\sigma}|d^\dagger_{l\sigma}\rangle\rangle^r \\ &\quad + U_j\langle\langle d_{j\sigma} n_{j\bar\sigma}|d^\dagger_{l\sigma}\rangle\rangle^r . \end{aligned} \tag{6}$$

Here the notation $z = \omega + \mathrm{i}0^+$ is used, $\Gamma_{11} = (\Gamma^L_{11} + \Gamma^R_{11})/2$, and $\Gamma_{22} = \Gamma^D/2$. In the above equation, besides the Green functions $\langle\langle d_{j\sigma}|d^\dagger_{l\sigma}\rangle\rangle^r$ and $\langle\langle d_{j\pm1\sigma}|d^\dagger_{l\sigma}\rangle\rangle^r$ with which we are concerned, a new Green function $\langle\langle d_{j\sigma} n_{j\bar\sigma}|d^\dagger_{l\sigma}\rangle\rangle^r$ is inevitably involved. We thus need to work out its equation of motion further. However, because of the many-body terms in the Hamiltonian, we have to truncate the equations of motion at some order to form a closed set of equations. We arrive at the second-order approximation, which is to truncate the equations of motion of the Green function $\langle\langle d_{j\sigma} n_{j\bar\sigma}|d^\dagger_{l\sigma}\rangle\rangle^r$ in the following way:

$$\begin{aligned} &(z - \varepsilon_j - U_j)\langle\langle d_{j\sigma} n_{j\bar\sigma}|d^\dagger_{l\sigma}\rangle\rangle^r \\ &= \langle n_{j\bar\sigma}\rangle\delta_{jl} + t_{j-1}(1-\delta_{j1})\langle n_{j\bar\sigma}\rangle\langle\langle d_{j-1\sigma}|d^\dagger_{l\sigma}\rangle\rangle^r \\ &\quad + t^*_j(1-\delta_{j2})\langle n_{j\bar\sigma}\rangle\langle\langle d_{j+1\sigma}|d^\dagger_{l\sigma}\rangle\rangle^r \\ &\quad - \mathrm{i}\Gamma_{jj}\langle n_{j\bar\sigma}\rangle\langle\langle d_{j\sigma}|d^\dagger_{l\sigma}\rangle\rangle^r . \end{aligned} \tag{7}$$

In Eq. (7) the approximations $\langle\langle d_{1\sigma} n_{2\bar\sigma}|d^\dagger_{l\sigma}\rangle\rangle^r \approx \langle n_{2\bar\sigma}\rangle \times\langle\langle d_{1\sigma}|d^\dagger_{l\sigma}\rangle\rangle^r$ and $\langle\langle c_{k\sigma\alpha} n_{2\bar\sigma}|d^\dagger_{l\sigma}\rangle\rangle^r \approx \langle n_{2\bar\sigma}\rangle\langle\langle c_{k\sigma\alpha}|d^\dagger_{l\sigma}\rangle\rangle^r$

have been used to eliminate these high-order Green functions. The advantage of this approach is that it allows for an explicit expression about the linear conductance in terms of the equilibrium state Green functions, while the cost of such an approach is that the influence of electron correlation on the transport properties is left out, such as the Kondo effect.[17] However, if we focus on the conductance spectrum in the mixed-valence region, the Kondo effect and the other co-tunneling mechanism will only contribute to the spectrum trivially.

From the above equations, we can obtain the solution of the retarded Green function, which is written in a matrix form as

$$G^r_\sigma(\omega) = \begin{bmatrix} g^r_{1\sigma}(z)^{-1} & -t_1^* \\ -t_1 & g^r_{2\sigma}(z)^{-1} \end{bmatrix}^{-1}, \tag{8}$$

with

$$g^r_{j\sigma}(z) = \Big\{(z-\varepsilon_j)\frac{z-\varepsilon_j-U_j}{z-\varepsilon_j-U_j+U_j\langle n_{j\bar\sigma}\rangle} + \mathrm{i}\Gamma_{jj}\Big\}^{-1} \tag{9}$$

being the zero-order Green function of QD-j unperturbed by another QD. Here the average electron occupation number in QD is determined by the relations $\langle n_{j\sigma}\rangle = -(1/\pi)\int \mathrm{d}\omega\, \mathrm{Im}\, G^r_{jj,\sigma}$.

3 Numerical Results and Discussions

With the formulation developed in the previous section, we can perform the numerical calculation about the linear conductance spectrum of this double QD system. Thus the Fano effect in the presence of decoherence mechanism modeled by introducing a floating lead can be revealed. Prior to the calculation, we need to introduce a parameter t_0 as the unit of energy. The linear conductance is only related to the equilibrium state properties of the system, though the nonequilibrium Green function technique has been used to derive the expression about it. In equilibrium the system has a uniform Fermi energy and it is taken as the zero point of energy.

First of all, we focus on the characteristics of the linear conductance spectrum in the absence of electron interactions. This means $U_j = 0$ for all QDs. Here we choose the parameter values $t_1 = t_0$, $\varepsilon_1 = \varepsilon_0 + \Delta$, and $\varepsilon_2 = \varepsilon_0 - \Delta$ to perform the numerical calculation. Surely, ε_0 can be shifted with respect to the Fermi level by adjusting the gate voltage. And Δ can be fixed at different values, accordingly we firstly assume that it equals t_0. Then, we change Γ^D to study the conductance spectrum of the T-shaped QD structure with $\Gamma^L_{11} = \Gamma^R_{11} = \Gamma_0 = t_0$. The numerical results are shown in Fig. 2. From this figure we can firstly find that, in the absence of the lateral lead ($\Gamma^D = 0$), an apparent Fano effect appears indeed. It is just the result of the quantum interference. When the floating lead is introduced, the Fano lineshape then changes, which shows the distinct restraint of the Fano peak, even if a comparatively weak dot-lead coupling. And the destruction of the Fano resonance is more obvious with the increasing of Γ^D.

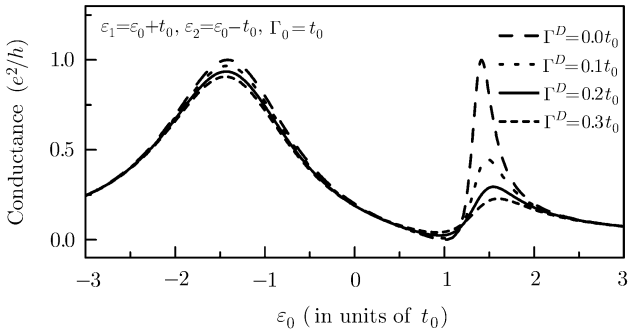

Fig. 2 The linear conductance spectra of the T-shaped double QD structure with the floating lead. Both of the QD levels are tuned by the gate voltage ($\varepsilon_1 = \varepsilon_0 + t_0$ and $\varepsilon_2 = \varepsilon_0 - t_0$). The dot-lead coupling $\Gamma_0 = t_0$. Γ^D is modulated to 0, $0.1t_0$, $0.2t_0$, and $0.3t_0$.

To clarify the above numerical results, we need to transform the coupled double QDs in the structure to its molecular orbital representation. Accordingly, the Hamiltonian is given by

$$h = h_c + h_d + h_t\,, \tag{10}$$

with

$$\begin{aligned} h_c &= \sum_{k\alpha\in L,R,D} \varepsilon_{k\alpha} c^\dagger_{k\alpha} c_{k\alpha}\,, \quad h_d = \sum_{j=1}^{2} e_j f^\dagger_j f_j\,, \\ h_t &= \sum_{kL,j}\Big(v_{jL} f^\dagger_j c_{kL} + \sum_{kR,j} v_{jR} f^\dagger_j c_{kR} \\ &\quad + \sum_{kD,j} v_{jD} f^\dagger_j c_{kD} + \mathrm{h.c.}\Big)\,. \end{aligned} \tag{11}$$

The mapping of the parameters is given as follows:

$$\begin{aligned} e_1 &= \frac{1}{2}\big(\varepsilon_1+\varepsilon_2 - \sqrt{(\varepsilon_1-\varepsilon_2)^2+4t_0^2}\,\big)\,, \\ e_2 &= \frac{1}{2}\big(\varepsilon_1+\varepsilon_2 + \sqrt{(\varepsilon_1-\varepsilon_2)^2+4t_0^2}\,\big)\,; \end{aligned} \tag{12}$$

and

$$\begin{aligned} v_{1\beta} &= \sqrt{\frac{t_0^2}{t_0^2+(e_1-\varepsilon_1)^2}}V_{1\beta}\,, \\ v_{2\beta} &= -\sqrt{\frac{t_0^2}{t_0^2+(e_2-\varepsilon_1)^2}}V_{1\beta}\,, \\ v_{1D} &= \sqrt{\frac{(e_1-\varepsilon_1)^2}{t_0^2+(e_1-\varepsilon_1)^2}}V_{2D}\,, \\ v_{2D} &= \sqrt{\frac{(e_2-\varepsilon_1)^2}{t_0^2+(e_2-\varepsilon_1)^2}}V_{2D}\,. \end{aligned} \tag{13, 14}$$

Here we need to define $[\gamma^\alpha]_{jn} = 2\pi v_{j\alpha} v^*_{n\alpha}\rho_\alpha(\omega)$ and $\gamma_{ij} = (\gamma^L_{ij} + \gamma^R_{ij} + \gamma^D_{ij})/2$. Considering that our purpose is

to study the Fano effect in the electron conductance spectrum, it is helpful to make a Feynman path analysis about the electron transmission process through the QDs.[19] It will be seen that the Feynman paths give an intuitive picture about quantum interference, which is just the underlying mechanism of the Fano effect. We start such an analysis by rewriting the electron transmission function as $T(\omega) = \mathrm{Tr}[\gamma^L \mathcal{G}^r \gamma^R \mathcal{G}^a] = |\sum_{j,l=1}^{2} t(j,l)|^2$, where the new Green functions $\mathcal{G}^r_{jl} = \langle\langle f_j | f_l^\dagger \rangle\rangle^r$ and the electron transmission coefficients are defined as $t(j,l) = \mathcal{V}_{Lj}\mathcal{G}^r_{jl}\mathcal{V}_{lR}$ with $\mathcal{V}_{j\alpha} = \mathcal{V}^*_{\alpha j} = v_{j\alpha}\sqrt{2\pi\rho_\alpha(\omega)}$ (Besides, we define $\tilde{v}_{j\alpha} = \tilde{v}^*_{\alpha j} = v_{j\alpha}\sqrt{\pi\rho_\alpha(\omega)}$ for the following discussion). Furthermore, the transmission coefficient, e.g., $t(1,1)$ is expressed as a summation of Feynman paths with different orders, i.e.,

$$\begin{aligned} t(1,1) &= \sum_{j=0}^{\infty} \mathcal{V}_{L1} g_1 (-g_1 g_2 \gamma_{12}\gamma_{21})^j \mathcal{V}_{1R} \\ &= \sum_{j=0}^{\infty} t_j(1,1)\,, \end{aligned} \tag{15}$$

with $g_j(z) = (z - e_j + \mathrm{i}\gamma_{jj})^{-1}$ here. For example, $t_0(1,1) = \mathcal{V}_{L1} g_1 \mathcal{V}_{1R}$ and

$$t_1(1,1) = -\mathcal{V}_{L1} g_1^2 g_2 \gamma_{12}\gamma_{21} \mathcal{V}_{1R}\,, \tag{16}$$

which consists of nine terms representing individual Feynman paths. They are denoted as

$$\begin{aligned} t_{1a}(1,1) &= -\mathcal{V}_{L1} g_1 \tilde{v}_{1L} \tilde{v}_{L2} g_2 \tilde{v}_{2L} \tilde{v}_{L1} g_1 \mathcal{V}_{1R}\,, \\ t_{1b}(1,1) &= -\mathcal{V}_{L1} g_1 \tilde{v}_{1L} \tilde{v}_{L2} g_2 \tilde{v}_{2R} \tilde{v}_{R1} g_1 \mathcal{V}_{1R}\,, \\ t_{1c}(1,1) &= -\mathcal{V}_{L1} g_1 \tilde{v}_{1R} \tilde{v}_{R2} g_2 \tilde{v}_{2L} \tilde{v}_{L1} g_1 \mathcal{V}_{1R}\,, \\ t_{1d}(1,1) &= -\mathcal{V}_{L1} g_1 \tilde{v}_{1R} \tilde{v}_{R2} g_2 \tilde{v}_{2R} \tilde{v}_{R1} g_1 \mathcal{V}_{1R}\,, \\ t_{1e}(1,1) &= -\mathcal{V}_{L1} g_1 \tilde{v}_{1L} \tilde{v}_{L2} g_2 \tilde{v}_{2D} \tilde{v}_{D1} g_1 \mathcal{V}_{1R}\,, \\ t_{1f}(1,1) &= -\mathcal{V}_{L1} g_1 \tilde{v}_{1R} \tilde{v}_{R2} g_2 \tilde{v}_{2D} \tilde{v}_{D1} g_1 \mathcal{V}_{1R}\,, \\ t_{1g}(1,1) &= -\mathcal{V}_{L1} g_1 \tilde{v}_{1D} \tilde{v}_{D2} g_2 \tilde{v}_{2R} \tilde{v}_{R1} g_1 \mathcal{V}_{1R}\,, \\ t_{1h}(1,1) &= -\mathcal{V}_{L1} g_1 \tilde{v}_{1D} \tilde{v}_{D2} g_2 \tilde{v}_{2L} \tilde{v}_{L1} g_1 \mathcal{V}_{1R}\,, \\ t_{1i}(1,1) &= -\mathcal{V}_{L1} g_1 \tilde{v}_{1D} \tilde{v}_{D2} g_2 \tilde{v}_{2D} \tilde{v}_{D1} g_1 \mathcal{V}_{1R}\,. \end{aligned} \tag{17}$$

We can find that introducing the floating lead brings latter five paths. The higher-order Feynman paths have more complicated forms. In the same way, $t(1,2)$ can also be divided into a summation of Feynman paths. It is given by

$$\begin{aligned} t(1,2) &= \sum_{j=1}^{\infty} \mathrm{i}\mathcal{V}_{L1} (-g_1 g_2 \gamma_{12})^j \gamma_{21}^{j-1} \mathcal{V}_{2R} \\ &= \sum_{j=1}^{\infty} t_j(1,2)\,, \end{aligned} \tag{18}$$

and there are three different lowest-order Feynman paths in $t(1,2)$, they are,

$$\begin{aligned} t_{1a}(1,2) &= -\mathrm{i}\mathcal{V}_{L1} g_1 \tilde{v}_{1L} \tilde{v}_{L2} g_2 \mathcal{V}_{2R}\,, \\ t_{1b}(1,2) &= -\mathrm{i}\mathcal{V}_{L1} g_1 \tilde{v}_{1R} \tilde{v}_{R2} g_2 \mathcal{V}_{2R}\,, \\ t_{1c}(1,2) &= -\mathrm{i}\mathcal{V}_{L1} g_1 \tilde{v}_{1D} \tilde{v}_{D2} g_2 \mathcal{V}_{2R}\,. \end{aligned} \tag{19}$$

$t_{1c}(1,2)$ is from the introducing of floating lead. The other two transmission coefficients $t(2,2)$ and $t(2,1)$ have the similar expansions as $t(1,1)$ and $t(1,2)$. Obviously, the introducing of the floating lead complicates the quantum interference.

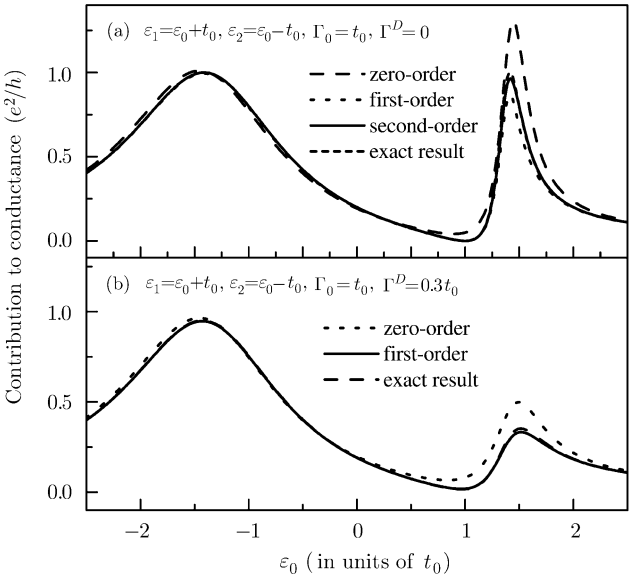

Fig. 3 The linear conductance spectra calculated by the approximations up to different order Feynman paths. (a) The zero-, first-, and second-order approximations in the absence of the dot-floating-lead coupling. (b) The zero- and first-order approximations for the case of $\Gamma^D = 0.3t_0$.

The above analysis is very helpful for us to explain the distinctly different influences of the floating lead on the Fano lineshape shown in Fig. 2. Surely, the Fano lineshape should be considered as the result of interference among electron waves passing through infinite-order Feynman paths. But it can be anticipated that only the low-order paths play the predominant roles to the conductance spectrum. In Fig. 3, we give a comparison of the exact linear conductance spectrum with those results calculated with only some low order Feynman paths. By comparing the spectra shown in Fig. 3, we can conclude that the emergence of the floating lead results in the higher-order Feynman paths unimportance. For example, when Γ^D takes moderate values the calculated results within the first-order approximation is very close to the exact conductance spectrum, which is clearly shown in Fig. 3(b). Among all the Feynman paths, $t_0(1,1)$ and $t_0(2,2)$, the two lowest-order paths are certainly the most important contributions to the Fano lineshape. In Fig. 4(a) we plot the contributions of these two paths. We can find that by altering Γ^D, $t_0(2,2)$ presents notable variation which predominantly contributes to the Fano resonance region. On the other hand, $t_0(1,1)$ does not change in principle with

the increase of Γ^D. Furthermore, we can check the contributions of other low-order paths. In Fig. 4(b) $|t_1(1,1)|^2$ is shown with the different Γ^D. Besides, in Figs. 4(c) and 4(d), $|t_1(1,2)|^2$ and $|t_1(2,2)|^2$ are shown, respectively. We can realize that they depend on Γ^D sensitively. Up to now the variation of the Fano lineshape relative to the increase of the coupling of QD to the floating lead, as shown in Fig. 2, has been well explained by analyzing the contributions of the predominant Feynman paths.

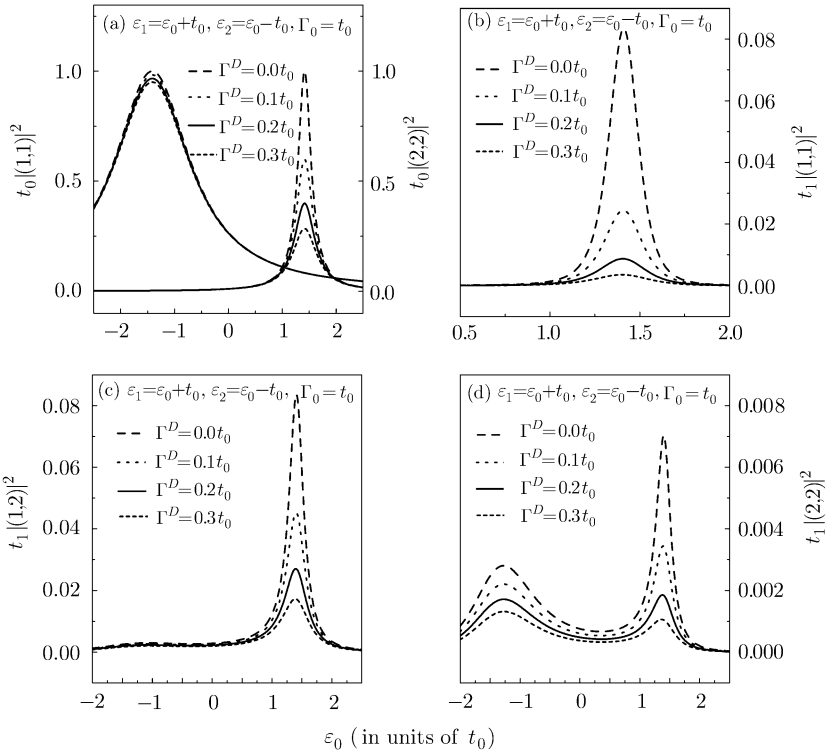

Fig. 4 The contributions of the leading Feynman paths to the electron transmission function. (a) The contributions of the zero-order Feynman paths corresponding to the increase of Γ^D. (b) The contributions of $t_1(1,1)$ with the adjusting of Γ^D. (c) and (d) The contributions of $t_1(1,2)$ and $t_1(2,2)$ in the case of adjusting Γ^D, respectively.

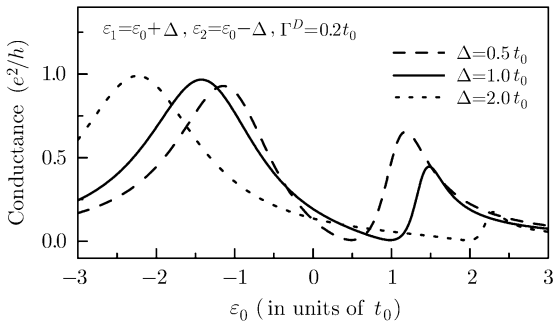

Fig. 5 The linear conductance spectra of the T-shaped double QD structure. The structure parameters take the following values: $\varepsilon_1 = \varepsilon_0 + \Delta$ and $\varepsilon_2 = \varepsilon_0 - \Delta$; The dot-lead coupling $\Gamma_0 = t_0$ and $\Gamma^D = 0.2t_0$. $\Delta = 0.5t_0$, t_0, and $2.0t_0$, respectively.

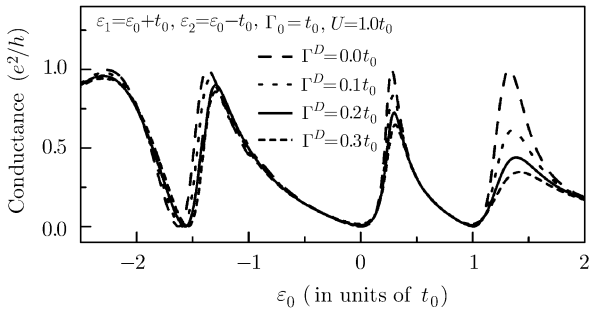

Fig. 6 The linear conductance spectra of the T-shaped double QD structure. The many-body effect is incorporated to the second order approximation. The parameter values are $U_j = U = 1.0t_0$, $\varepsilon_1 = \varepsilon_0 + t_0$, $\varepsilon_2 = \varepsilon_0 - t_0$, and $\Gamma_0 = t_0$.

On the other hand, by fixing $\Gamma^D = 0.2t_0$ and letting Δ correspond to different values, we obtain the conductance spectra in Fig. 5. Here we can find that the Fano lineshape can be changed remarkably with increasing Δ. This phenomenon can be understood as follows. The increment of Δ causes Fano lineshape more apparent than the case of small Δ, then the contributions of different order Feynman paths in the Fano region would become little for the same coupling strength between the dangling QD and the floating lead.

Now we incorporate the electron interaction terms into the calculation of the linear conductance spectrum. We assume $U_j = U = t_0$ and truncate the equations of motion of Green functions to the second-order approximation following the description in the previous section. Figure 6 shows the linear conductance spectra. From the figure we can find that two Fano peaks appear in the conductance spectrum, due to the Coulomb repulsion. In such a case, the energy level of QD-2 splits into two: ε_2 and ε_2+U, the zero values of which still corresponds to the antiresonant points. In addition, another antiresonance occurs at $\varepsilon_0 \approx -1.5t_0$, which just corresponds to the electron-hole symmetry case for QD-1 with $\varepsilon_1 = -U/2$.[15] However, the main features found in the noninteracting case remain, i.e., the Fano region is drastically influenced by the floating lead. Therefore, we can conclude that the intra-dot Coulomb repulsion cannot change the decoherence effect in principle. Of course, we only consider the many-body effect to the mixed-valence. Then, one can pay attention to the influence of Kondo resonance on this structure. Such an interesting topic is beyond the scope of the present work, and will be left for future study.

4 Summary

By means of a generalized Anderson impurity Hamiltonian, we have investigated the electronic transport through a T-shaped double quantum dot system. The Fano lineshape appears in the linear conductance spectrum of this structure. While introducing the floating lead coupled to the lateral QD, the influence of the decoherence mechanism on the Fano lineshape is studied. We would like to emphasize two points concerning our results. First, we find that the floating lead coupled to the lateral QD plays a crucial role in destroying the Fano lineshape. Secondly, the decoherence mechanism inhibits the contributions of the high order Feynman paths to the conductance spectrum. This result implies that an approximate approach with only the low-order paths included can give a quantitative description of the conduction spectrum.

References

[1] U. Fano, Phys. Rev. **124** (1961) 1866.

[2] K. Kobayashi, H. Aikawa, S. Katsumoto, and Y. Iye, Phys. Rev. Lett. **88** (2002) 256806; Phys. Rev. B **68** (2003) 235304; M. Sato, H. Aikawa, K. Kobayashi, S. Katsumoto, and Y. Iye, Phys. Rev. Lett. **95** (2005) 066801; K. Kobayashi, H. Aikawa, A. Sano, S. Katsumoto, and Y. Iye, Phys. Rev. B **70** (2003) 035319.

[3] J. Göres, D. Goldhaber-Gordon, S. Heemeyer, and M.A. Kastner, Phys. Rev. B **62** (2000) 2188.

[4] I.G. Zacharia, D. Goldhaber-Gordon, G. Granger, M.A. Kastner, Y.B. Khavin, H. Shtrikman, D. Mahalu, and U. Meirav, Phys. Rev. B **64** (2001) 155311.

[5] B.R. Bułka and P. Stefański, Phys. Rev. Lett. **86** (2001) 5128.

[6] B. Kubala and J. König, Phys. Rev. B **65** (2002) 245301.

[7] K. Kang and S.Y. Cho, J. Phys.: Condens. Matter **16** (2004) 117; Z.M. Bai, M.F. Yang, and Y.C. Chen, J. Phys.: Condens. Matter **16** (2004) 4303.

[8] M.L. Ladron de Guevara, F. Claro, and P.A. Orellana, Phys. Rev. B **67** (2003) 195335.

[9] H. Lu, R. Lü, and B.F. Zhu, Phys. Rev. B **71** (2005) 235320.

[10] A.A. Clerk, X. Waintal, and P.W. Brouwer, Phys. Rev. Lett. **86** (2001) 4636.

[11] L. Liu, Y. Du, H. Zhou, and T. Lin, Phys. Rev. B **54** (1996) 1953.

[12] A. Ueda and M. Eto, Phys. Rev. B **73** (2006) 235353.

[13] J. König and Y. Gefen, Phys. Rev. Lett. **86** (2001) 3855; Phys. Rev. B **65** (2002) 045316.

[14] M. Buttiker, Phys. Rev. Lett. **57** (1986) 1761; H.Q. Xu, Appl. Phys. Lett. **78** (2001) 2064.

[15] W. Gong, Y. Zheng, Y. Liu, and T. Lü, Phys. Rev. B **73** (2006) 245329.

[16] Y. Liu, Y. Zheng, W. Gong, and T. Lü, Phys. Lett. A **365** (2007) 495.

[17] Y. Meir and N.S. Wingreen, Phys. Rev. Lett. **68** (1992) 2512; A.P. Jauho, N.S. Wingreen, and Y. Meir, Phys. Rev. B **50** (1994) 5528.

[18] C. Niu, D.L. Lin, and T.H. Lin, J. Phys.: Condens. Matter **11** (1999) 1511.

[19] S. Datta, *Electron Transport in Mesoscopic Systems Cambridge University Press*, Cambridge, England (1997).